Release mode of large and small dense-core vesicles specified by different synaptotagmin isoforms in PC12 cells

Zhen Zhang[a,*], Yao Wu[a,b], Zhao Wang[a,b], F. Mark Dunning[a,b], Jonathan Rehfuss[a,b], Deepshika Ramanan[a,b], Edwin R. Chapman[a,b], and Meyer B. Jackson[a]
[a]Department of Physiology, University of Wisconsin School of Medical and Public Health, Madison, WI 53706;
[b]Howard Hughes Medical Institute, Chevy Chase, MD 20815

ABSTRACT **Many cells release multiple substances in different proportions according to the specific character of a stimulus. PC12 cells, a model neuroendocrine cell line, express multiple isoforms of the exocytotic Ca^{2+} sensor synaptotagmin. We show that these isoforms sort to populations of dense-core vesicles that differ in size. These synaptotagmins differ in their Ca^{2+} sensitivities, their preference for full fusion or kiss-and-run, and their sensitivity to inhibition by synaptotagmin IV. In PC12 cells, vesicles that harbor these different synaptotagmin isoforms can be preferentially triggered to fuse by different forms of stimulation. The mode of fusion is specified by the synaptotagmin isoform activated, and because kiss-and-run exocytosis can filter small molecules through a size-limiting fusion pore, the activation of isoforms that favor kiss-and-run will select smaller molecules over larger molecules packaged in the same vesicle. Thus synaptotagmin isoforms can provide multiple levels of control in the release of different molecules from the same cell.**

Monitoring Editor
Patrick Brennwald
University of North Carolina

Received: Feb 24, 2011
Revised: Apr 13, 2011
Accepted: Apr 26, 2011

INTRODUCTION

Neurons and endocrine cells release an extraordinary variety of chemical signals. Small, clear synaptic vesicles (SVs) generally contain low–molecular weight neurotransmitters, whereas neuropeptides are packaged in larger, dense-core vesicles (DCVs). However, both nerve terminals and endocrine cells nearly always copackage neuropeptides together with smaller neurotransmitters (Hokfelt *et al.*, 2000; Salio *et al.*, 2006). Packaging different classes of molecules into SVs and DCVs provides for an effective means of regulating their exocytosis independently. The different sensitivities of these compartments to different signals have been well documented (Verhage *et al.*, 1991; Bean *et al.*, 1994; Zhou and Misler, 1995; Hokfelt *et al.*, 2000), although the molecular and cellular basis remains unclear. Moreover, DCVs often contain multiple neuropeptides, which are released together during DCV exocytosis (Hokfelt *et al.*, 1994; Salio *et al.*, 2006). Neuropeptides can be sorted to different DCVs in the same cell (Fisher *et al.*, 1988; Sossin *et al.*, 1990; Perello *et al.*, 2008), and differential regulation of release of peptide hormones from the same type of endocrine cell has been reported (Childs *et al.*, 1987; McNeilly *et al.*, 2003). The nature of the factors that determine the selective release of different molecular signals from a given population of cells thus emerges as a fundamental question that must be clarified in order to understand the orchestration of complex neural and endocrine processes that depend on the coordinated release of multiple chemical signals.

Neurotransmitters and hormones can be released by two very different modes of exocytosis—kiss-and-run and full fusion. Kiss-and-run is a partial release mode in which vesicle content exits through a fusion pore. In this mode the size of the fusion pore limits the size of a molecule that can be released. By contrast, full fusion results in complete expulsion of all the molecules stored in a vesicle. DCVs of adrenal chromaffin cells contain catecholamines, nucleotides, and neuropeptides (Winkler *et al.*, 1986). Chromaffin cells can release catecholamine and neuropeptide nearly simultaneously from the same vesicle (Whim, 2006), but, depending on the form of stimulation, norepinephrine alone is released by kiss-and-run and norepinephrine

This article was published online ahead of print in MBoC in Press (http://www.molbiolcell.org/cgi/doi/10.1091/mbc.E11-02-0159) on May 5, 2011.

*Present address: National Institute of Neurological Disorders and Stroke, Bethesda, MD 20892.

Address correspondence to: Meyer Jackson (mbjackso@wisc.edu; MJackson@physiology.wisc.edu).

Abbreviations used: Cg, chromogranin; DCV, dense-core vesicle; GFP, green fluorescent protein; SNAP-25, synaptosome-associated protein of molecular mass 25 kDa; SNARE, soluble N-ethyl maleimide sensitive factor receptor; SV, synaptic vesicle; syt, synaptotagmin; syx, syntaxin; TIRF, total internal reflection fluorescence.

together with neuropeptides is released by full fusion (Fulop *et al.*, 2005). Costored ATP and insulin can also be differentially secreted by distinct release modes in pancreatic beta cells (MacDonald *et al.*, 2006). Thus, although the mode of exocytosis can control the release of costored molecules, there is still much to learn about the molecular basis for the choice between kiss-and-run and full fusion.

Synaptotagmin (syt) I resides on secretory vesicles, where it serves as a Ca^{2+} sensor for exocytosis (Augustine, 2001; Koh and Bellen, 2003; Chapman, 2008). There are at least 17 different syt isoforms (Craxton, 2007) with varied biochemical properties, and the functional significance of this diversity is a very active area of investigation (Marqueze *et al.*, 2000; Sudhof, 2002; Bhalla *et al.*, 2005, 2008; Hui *et al.*, 2005). Given the roles of many syt isoforms in various forms of regulated exocytosis, the diversity within this protein family offers an attractive mechanistic strategy for selectivity of release. The neuroendocrine PC12 cell line contains syt I, syt IV, syt VII, and syt IX (Vician *et al.*, 1995; Fukuda *et al.*, 2002; Zhang *et al.*, 2002; Tucker *et al.*, 2003; Wang *et al.*, 2005). syt I, IX, and VII can all drive Ca^{2+}-triggered membrane fusion (Bhalla *et al.*, 2008) but have distinct biochemical properties. For example, syt VII binds phosphatidylserine (PS)-containing liposomes much more tightly than syt I, and syt IX shows intermediate PS binding (Zhang *et al.*, 2010a). By contrast, syt IV is a negative regulator of exocytosis (Wang *et al.*, 2001) and inhibits membrane fusion induced by other syt isoforms (Bhalla *et al.*, 2008). All four of the PC12 cell syt isoforms localize to DCVs (Fukuda *et al.*, 2002, 2004; Wang *et al.*, 2003, 2005), but their roles in the regulation of DCV exocytosis remain unresolved.

To determine whether syt diversity can contribute to selectivity of release, we explored the functional capabilities of the endogenous syt isoforms of PC12 cells. Using immunogold electron microscopy and immunofluorescence, we found that syt isoforms sort to different-sized populations of DCVs. Using amperometry and total internal reflection fluorescence (TIRF) microscopy, we found that these populations undergo distinct forms of exocytosis with different modes of release. Furthermore, these populations differ in their sensitivity to inhibition by syt IV. These functional distinctions within populations of vesicles from the same cell thus provide a molecular mechanism for independent and selective control of secretion of multiple signaling molecules.

RESULTS

Localization of syt isoforms

PC12 cells express four syt isoforms. syt I and IX are abundant, and syt IV and VII are sparse (Tucker *et al.*, 2003; Ahras *et al.*, 2006; Zhang *et al.*, 2010b), but all have been detected on DCVs (Wang *et al.*, 2001, 2003, 2005; Fukuda *et al.*, 2002, 2004). To compare their localization we overexpressed each isoform as a pHluorin fusion construct in PC12 cells and used immunogold labeling with an antibody against green fluorescent protein (GFP) to locate the proteins using electron microscopy. For all four syt isoforms, >50% of the gold particles were on DCVs (Figure 1A). We saw 3.7 ± 0.5, 3.4 ± 0.6, 3.4 ± 0.7, and 3.9 ± 0.7 particles per labeled DCV for syt I, syt IV, syt VII, and syt IX, respectively. These numbers are probably slight underestimates because in vesicles labeled with many particles counting was difficult due to overlap. The percents of labeled vesicles were 46, 40, 54, and 47%, respectively, for these four isoforms. According to the Poisson distribution there would be only ~3% unlabeled DCVs with a mean of 3.5 particles. Thus unlabeled DCVs appear to have little if any of the targeted isoform. This indicates that DCVs harboring a specific isoform were efficiently labeled. The absence of targeted protein from many DCVs supports the specificity of labeling and further argues against the spillover of overexpressed protein into compartments that do not normally express a particular syt isoform.

We analyzed the diameters of DCVs harboring different syt isoforms and found mean diameters of 108.1 ± 2.6, 129.1 ± 5.5, 148.1 ± 4.0, and 130.2 ± 4.0 nm for DCVs bearing syt I, IV, VII, and IX, respectively (N = 54–140; Figure 1, B–E, shows the size distributions, and Figure 1F shows the mean diameters). Thus syt I preferentially localizes to small DCVs, syt IV and IX to intermediate-sized DCVs, and syt VII to large DCVs (Figure 1H). The overexpression of each syt isoform failed to alter the average DCV size in PC12 cells (Figure 1G), indicating that the immunogold labeling revealed differential targeting rather than an effect of overexpressing different isoforms on vesicle size.

To explore the functional consequences of this differential localization we exploited the result that in liposome fusion assays syt isoforms differ in their divalent cation sensitivities (Bhalla *et al.*, 2005). Using amperometry to detect norepinephrine release from PC12 cells, we triggered exocytosis with Ca^{2+}, Sr^{2+}, or Ba^{2+}. With each divalent cation the shapes of the unitary events varied (Figure 2A shows three selected events, and Supplemental Figure S1 shows the mean rise times, decay times, and widths at half-height). With exocytosis triggered by Ca^{2+}, single-vesicle amperometric spikes rose and fell more rapidly, Sr^{2+}-triggered events rose and fell with intermediate speed, and Ba^{2+}-triggered events were the slowest. In terms of total area (total norepinephrine detected per unitary event) Ba^{2+}-evoked events were the largest (75.6 ± 2.9 pA*ms), Sr^{2+}-evoked events were intermediate (64.9 ± 1.8 pA*ms) (Figure 2B), and Ca^{2+}-evoked events were the smallest (50.2 ± 1.5 pA*ms). Distributions of areas of events evoked by each metal confirm this overall trend and show some overlap (Figure 2C). DCV size and content have been shown to change in parallel (Gong *et al.*, 2003), and the distribution of total amperometric spike area is nearly superimposable on the distribution of DCV size in both PC12 cells and chromaffin cells (Zhang and Jackson, 2010). Our results thus indicate that each divalent cation preferentially triggers exocytosis of different-sized DCVs. Ba^{2+} triggers the exocytosis of larger DCVs, Sr^{2+} triggers the exocytosis of intermediate-sized DCVs, and Ca^{2+} triggers the exocytosis of smaller DCVs.

To relate the sizes of different syt isoform–bearing DCVs to the variation in norepinephrine content per vesicle for the different divalent cations, we performed liposome fusion assays. Previous studies of syt cation specificity used liposomes composed of only phosphatidylcholine (PC) and PS (Bhalla *et al.*, 2005). Because phosphatidylethanolamine (PE) enhances the efficiency of liposome fusion (Gaffaney *et al.*, 2008), and PC12 cells contain PE (Ariga *et al.*, 1988; Zhang *et al.*, 2009b), we added this phospholipid to the liposomes in our fusion assay (see *Materials and Methods*). We first assayed syt I, VII, and IX because these isoforms promote fusion, whereas syt IV inhibits fusion (Bhalla *et al.*, 2008). (Note that all of the experiments performed here used the syt cytoplasmic domain because liposome fusion assays with full-length proteins are technically difficult.) Ba^{2+} stimulated only syt VII–mediated fusion, with a half-maximal effect ($[Ba^{2+}]_{½}$) at 298 µM (Figure 2, D and E, and Table 1). Among the syt isoforms endogenous to PC12 cells, only syt VII can transduce a Ba^{2+} signal for exocytosis. This indicates that it is likely that this protein serves as the Ba^{2+} sensor for exocytosis in PC12 cells. The result from the fusion assay thus links our results on vesicle size with our results from amperometry. The fact that Ba^{2+} triggers exocytosis of DCVs that contain a larger amount of norepinephrine (Figure 2, A–C) is consistent with the localization of syt VII on larger DCVs (Figure 1).

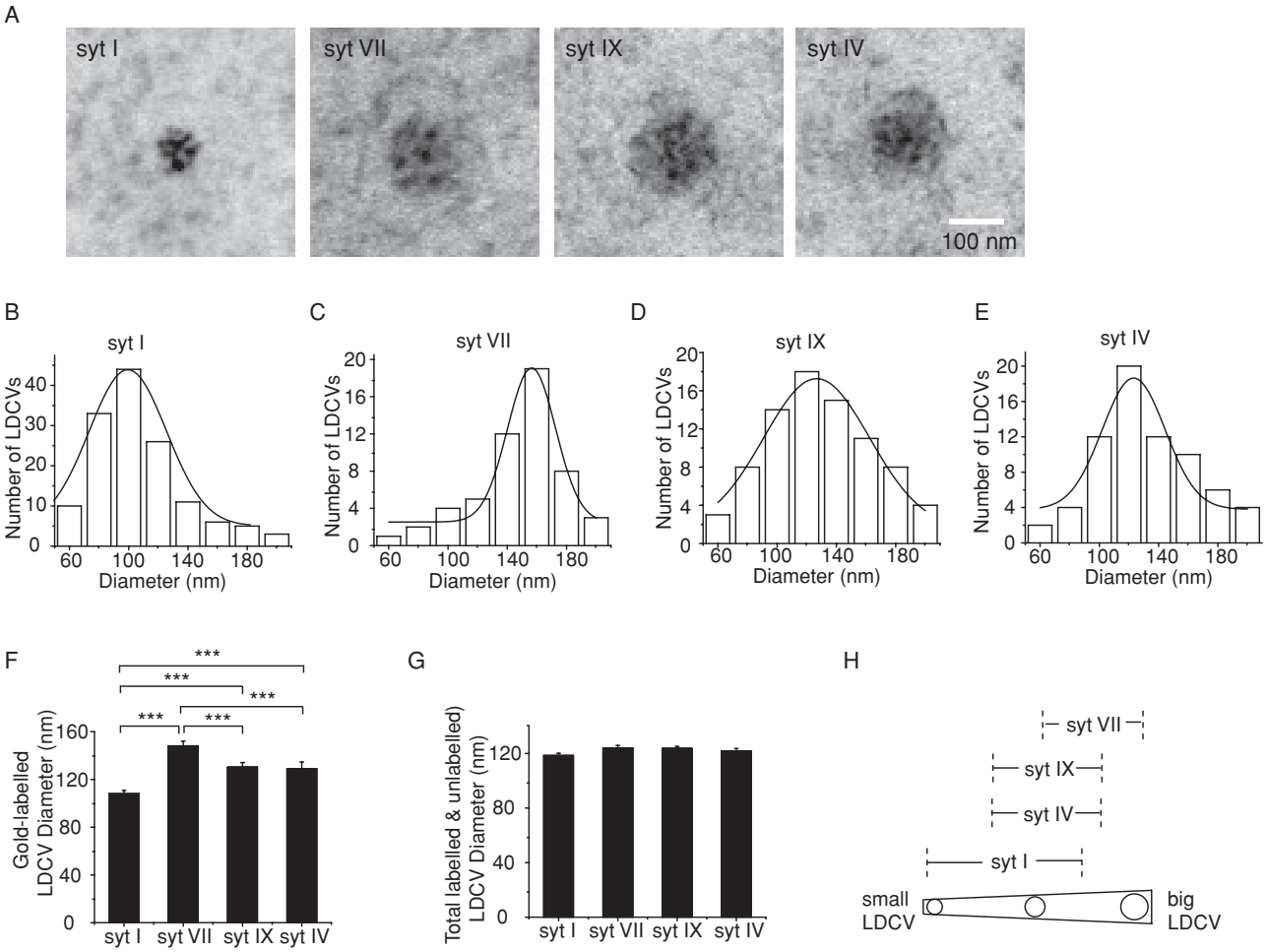

FIGURE 1: Localization of syt isoforms on DCVs by immunogold electron microscopy. (A) Sample images for syt I, VII, IX, and IV localization. Distributions of diameters of DCVs labeled with gold particles coupled to syt I–pHluorin (B), syt VII-pHluorin (C), syt IX–pHluorin (D), and syt IV–pHluorin (E) show that syt isoforms target DCVs of different sizes. Each distribution was fitted to a Gaussian function. (F) The mean diameter determined as the peak of the distribution differs significantly between all pairs except syt IV and syt IX. (G) DCV sizes were not changed by overexpression of syt isoforms. (H) Diagram summarizing the DCV size preferences of syt isoforms. From 178 to 374 DCVs were measured for each syt isoform. Error bars represent SEM; ***$p < 0.001$.

Sr^{2+} stimulated fusion mediated by both syt VII and syt IX, with $[Sr^{2+}]_{½}$ values of 68.2 and 435 μM, respectively (Figure 2, F and G, and Table 1), but Sr^{2+} failed to trigger fusion in the presence of syt I. Thus, if both syt VII and syt IX serve as Sr^{2+} sensors for exocytosis in PC12 cells, we can explain the smaller size of Sr^{2+}-triggered unitary events compared with Ba^{2+}-triggered unitary events (Figure 2, A–C) as a result of triggering the population of intermediate-sized, syt IX–labeled vesicles together with the population of large, syt VII–labeled vesicles (Figure 1). In spite of the clear results of the in vitro fusion assay, we cannot rule out some contribution of syt I to exocytosis triggered by Sr^{2+}, especially since Sr^{2+}-induced release was impaired in synapses of syt I knockout mice (Shin *et al.*, 2003). It is possible that the metal sensitivity in vivo and in cells does not mirror that in vitro, but it is also possible that the syt I knockout mouse leads to secondary deficits in the synaptic release apparatus such as reduced vesicle docking.

Finally, we found that Ca^{2+} triggered fusion with liposomes containing syt I, VII, or IX, with $[Ca^{2+}]_{½}$ values of 150.6, 0.93, and 5.8 μM, respectively (Figure 2, H and I, and Table 1), suggesting that all three of these isoforms can serve as Ca^{2+} sensors. The size of unitary amperometric events triggered by Ca^{2+} was the smallest of the three divalent cations tested, and this result is consistent with including the smallest syt I–bearing DCVs (Figure 2J). These experiments thus provide broad support for a functional role in the sorting of syt isoforms to different-sized DCVs. Because the functional experiments depend on endogenous protein, these results further suggest that both native and overexpressed syt–pHluorin constructs have similar DCV size preferences.

We next examined colocalization of the four syt isoforms using immunofluorescence microscopy in PC12 cells double labeled with antibodies against syt I, c-myc (c-myc–syt VII), syt IX, and syt IV (Figure 3A). Quantitative analysis (of images acquired with the same camera and microscope settings) revealed significant colocalization of each pair of syt isoforms (Figure 3D). For most pairs colocalization exceeded 60%. However, syt 1/syt VII colocalization was ~45%, similar to the result in a previous report (Wang *et al.*, 2005) and significantly lower than for the other pairs of syt isoforms ($p = 0.03$). This difference may reflect spatial segregation of different DCV populations, perhaps on the basis of size (Figure 1), as well as the presence of syt VII on lysosomes (Martinez *et al.*, 2000; Wang *et al.*, 2005). Low colocalization between syt isoforms and the non-DCV protein syntaxin served as a negative control (colocalization <10%) (Figure 3,

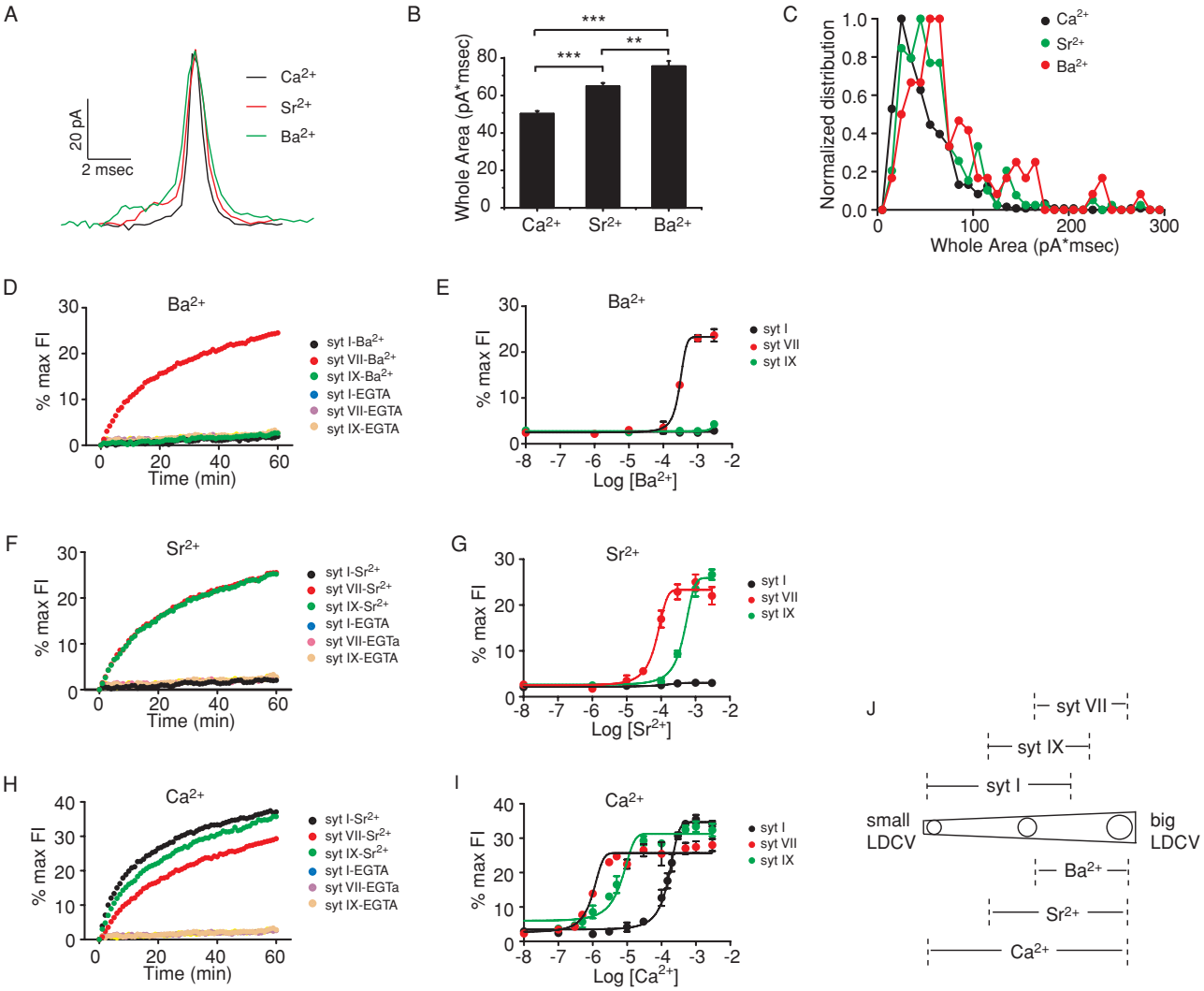

FIGURE 2: Norepinephrine release and liposome fusion triggered by divalent cations. (A) Sample amperometric spikes triggered by Ca^{2+}, Sr^{2+}, and Ba^{2+}. (B) Total spike areas differed for each divalent cation. (C) Distributions of spike areas for each metal. The different positions of the peaks parallel the different means in B. (D) syt I, VII, and IX differed in their stimulation of liposome fusion in response to 1 mM Ba^{2+}. (E) Plot of fusion vs. $[Ba^{2+}]$ for each isoform. (F, G) As in D and E, but with Sr^{2+}. (H, I) As in D and E, but with Ca^{2+}. (J) Diagram depicting the localization of syt isoforms on DCVs with various sizes from Figure 1 and DCVs for which exocytosis can be triggered by distinct divalent cations. For amperometry 320–1083 spikes were recorded from 62–80 cells, and for fusion assays at least three independent experiments were performed for each divalent cation. Error bars represent SEM; $^{**}p < 0.01$; $^{***}p < 0.001$.

B and D), and high colocalization between the DCV marker chromogranin B (Cg II) and the syt isoforms served as a positive control (colocalization ~60%) (Figure 3, C and D). Thus, to varying extents, the syt isoforms colocalize either on DCVs in the same regions of a cell or on the same DCVs.

syt isoform	EC_{50} Ca^{2+} (μM)	EC_{50} Sr^{2+} (μM)	EC_{50} Ba^{2+} (μM)
syt I	150.6 ± 15.8	n.d.	n.d.
syt VII	0.93 ± 0.31	68.2 ± 30.2	298.0 ± 19.9
syt IX	5.8 ± 2.4	435.2 ± 54.8	n.d.

EC_{50} values were determined from fusion assays in which percent maximum fluorescence was plotted vs. divalent cation concentration (see Figure 2). n.d., not determined.

TABLE 1: Half maximal effective concentration (EC_{50}) of divalent cation–stimulated membrane fusion.

Release mode of DCVs bearing distinct syt isoforms

To explore the functional implications of syt isoform sorting to different-sized DCVs in greater depth we used TIRF microscopy to investigate the mode of exocytosis in cells overexpressing different syt–pHluorin constructs. TIRF reports the exocytosis of an individual DCV as a rise in fluorescence as the pH-sensitive pHluorin experiences a change in environment from the low-pH vesicle lumen to the neutral-pH extracellular solution. GFP-tagged cargoes have shown similar pH-related fluorescence changes during DCV exocytosis in PC12 cells (Michael *et al.*, 2004; Taraska and Almers, 2004; Zhu *et al.*, 2007), PC12 cell sheets (Holroyd *et al.*, 2002), and pancreatic MIN6 β-cells (Tsuboi and Rutter, 2003). Examples of TIRF signals associated with single-vesicle exocytosis are illustrated for syt I– and syt VII–pHluorin (Figures 4, A–C). These three traces illustrate three distinct classes of events. In some events the fluorescence decays rapidly (Figure 4A), in some it decays slowly (Figure 4B), and in some the fluorescence remains high with no sign of decay during the

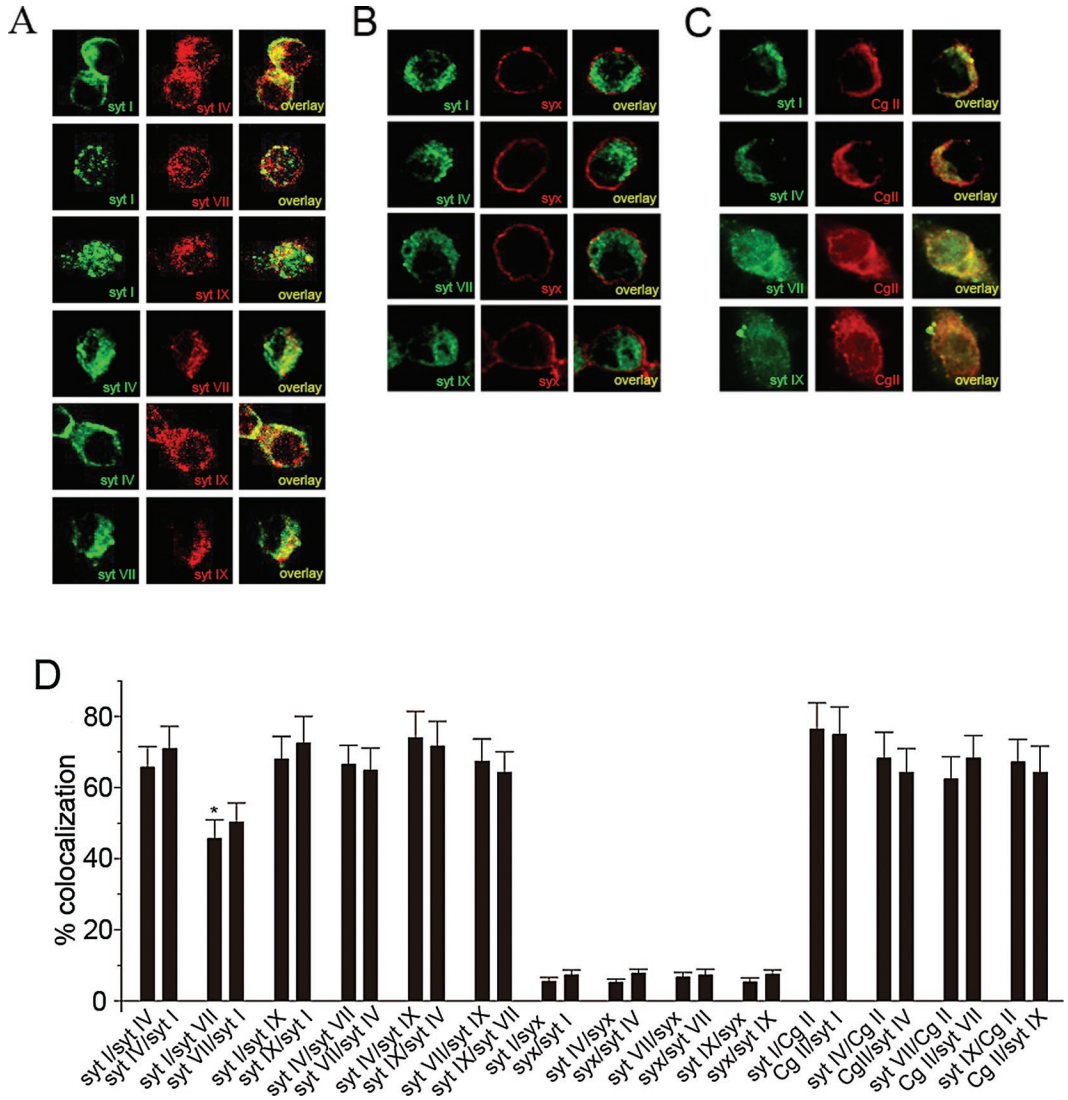

FIGURE 3: Protein–protein colocalization. (A) Fluorescence micrographs show colocalization of syt isoforms with one another. Each row shows localization of two different isoforms (left and center) together with colocalization as an overlay of the two images (right). (B) Colocalization of syt isoforms with syntaxin (syx). Each row shows syt isoform (left), syntaxin (center), and an overlay (right). (C) Colocalization of syt isoforms with chromogranin B (Cg II). Each row shows a syt isoform (left), Cg II (center), and an overlay (right). (D) Quantitative measures of colocalization were determined using ImageJ (see *Materials and Methods*) by analyzing overlay images such as shown in A–C, right. *$p < 0.05$ for syt I/syt VII against all other syt pairs except syt VII/syt I. All plotted values were based on three or more experiments.

duration of the recording (Figures 4C). These three modes had been noted previously in PC12 cells using TIRF of a content label (Zhu *et al.*, 2007). Supplemental Movies S1 and S2 illustrate two of these classes.

The slowly decaying and rapidly decaying events were evident as peaks in the decay time distributions for DCVs expressing each of the four syt–pHluorin constructs (Figure 4, D–G). With three of these constructs, syt I–pHluorin, syt IX–pHluorin, and syt IV–pHluorin, rapidly and slowly decaying events dominated, whereas persistent events were rare. By contrast, syt VII–pHluorin produced mostly slowly decaying and persistent events, whereas rapidly decaying events were rare. To relate these different classes of events to the mode of exocytosis, we increased the HEPES concentration from 10 to 100 mM. This increases the H^+ buffer capacity and slows the rate of reacidification of vesicles in neurons (Gandhi and Stevens, 2003) and astrocytes (Bowser and Khakh, 2007). We therefore expect a slower fluorescence decay for DCVs that reseal rapidly as occurs during kiss-and-run. With syt I–pHluorin, 100 mM HEPES prolonged decay times, moving the peak of rapidly decaying events to the right so that it nearly overlapped with the slowly decaying component seen in 10 mM HEPES (Figure 4H). With syt VII–pHluorin, 100 mM HEPES nearly eliminated the events with decays <2 s and left the slowly decaying peak essentially unchanged (Figure 4I). The sensitivity of the rapidly decaying component to 100 mM HEPES supports the view that these events reseal rapidly and are likely to be kiss-and-run. The events with long decay times in 10 mM HEPES then represent full fusion, and their slower fluorescence decay reflects diffusion of syt–pHluorin within the plasma membrane out of the region of interest. In 100 mM HEPES the kiss-and-run events decayed almost as slowly as full-fusion events and the decay time distribution did not afford a clear distinction between them. On the basis of the effect of elevated HEPES, we conclude that the rapid

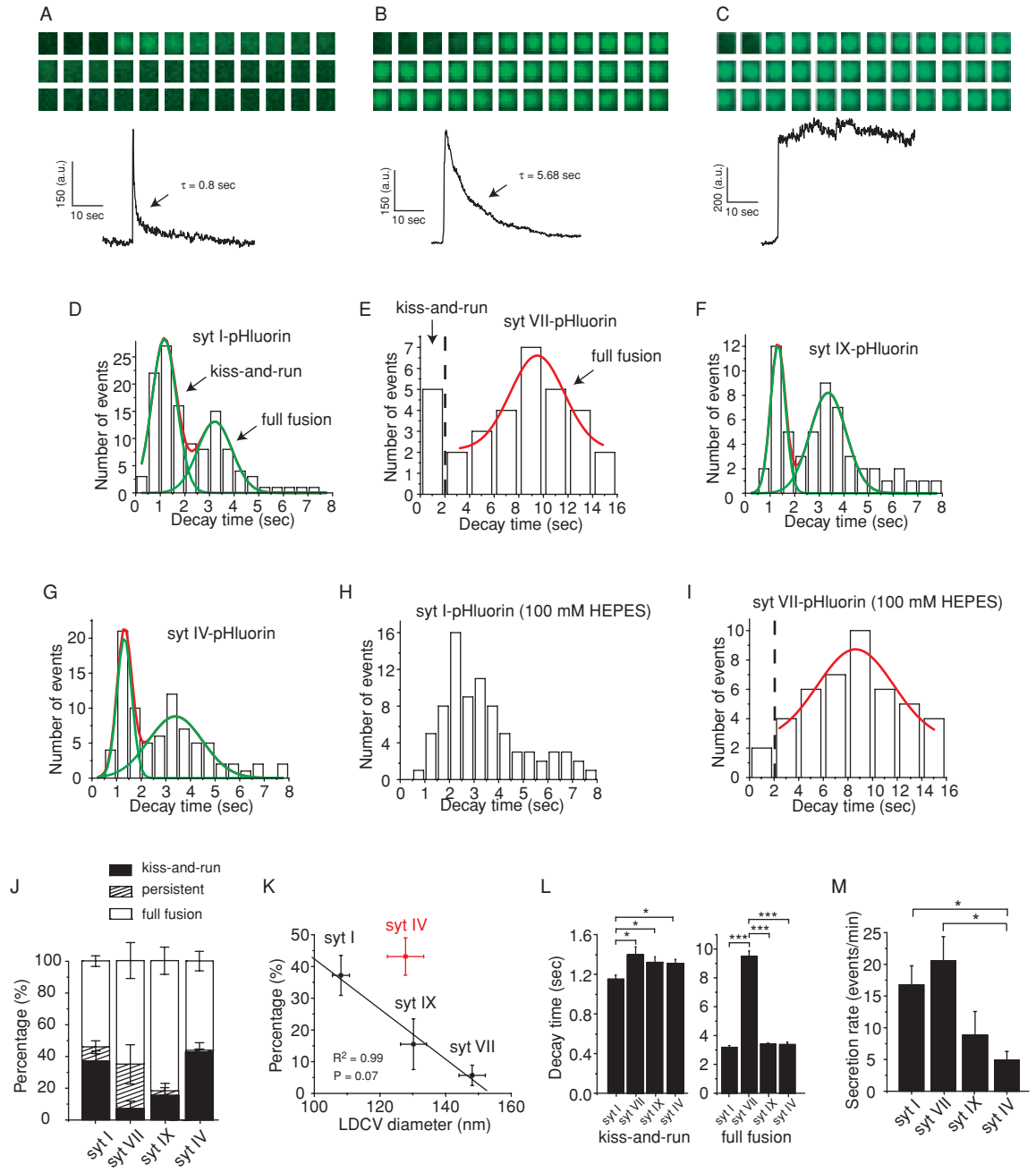

FIGURE 4: Total internal reflection fluorescence changes during exocytosis. (A–C) Three sample traces of unitary release events, with a sequence of images (at 100-ms intervals) from the release site above and fluorescence in these 1- to 2-μm regions of interest below. The examples shown from a PC12 cell transfected with syt I–pHluorin (A and B) and from a PC12 cell transfected with syt VII–pHluorin (C) show strikingly different time courses. (D) Decay times were determined from the fluorescence traces from PC12 cells transfected with syt I–pHluorin. The distribution of decay times revealed two peaks. (E) Decay-time distribution for cells transfected with syt VII–pHluorin shows longer decay times with only a few fast events corresponding to the peak at brief times in D. (F, G) Decay time distribution for cells transfected with syt IX–pHluorin and syt IV–pHluorin, respectively. (H) Decay-time distribution from syt I-pHluorin–transfected cells in 100 mM HEPES shows that the fast component of decay times seen in 10 mM HEPES became slower. (I) High HEPES similarly eliminated the small number of rapidly decaying events in cells transfected with syt VII–pHluorin but did not shift the peak at slowly decaying times. (J) Events were classified according to decay time as kiss-and-run (decay time <2 s), full fusion (decay time finite but >2 s), or persistent (no apparent decay), and the percentages were plotted for the different isoforms. syt VII produced the fewest kiss-and-run events, syt IX had an intermediate number, and syt I and syt IV produced the most. (K) The effect of the positive regulators of exocytosis (syt I, VII, and IX) on kiss-and-run decreased with the diameter of DCVs harboring that isoform (from Figure 1). The negative regulator (syt IV) fell off the fitted line for the positive regulators. (L) Mean decay times of kiss-and-run events and full-fusion events for each isoform. (M) Mean secretion rate (events/minute) from PC12 cells transfected with each syt isoforms. From 53 to 131 events were used for decay time analysis and 87–262 events for secretion rate analysis for recordings from 7–19 cells. Error bars represent SEM. *p < 0.05; **p < 0.01; ***p < 0.001.

decays reflect DCV reacidification. The ~1-s decay time of these events is considerably shorter than the 4- to 5-s decay constants seen for synaptic vesicle reacidification (Atluri and Ryan, 2006), suggesting that DCVs have a higher density of v-ATPase or a weakly buffered lumen.

We also saw variable numbers of persistent events, which probably reflect full fusion, but with the syt–pHluorin remaining clustered at the release site (Willig *et al.*, 2006). The present analysis will focus primarily on the rapidly and slowly decaying events. On the basis of the positions of the two peaks in the decay time distribution in 10 mM HEPES, we used 2 s as a cutoff, classifying faster events as kiss-and-run and slower events as full fusion. By this criterion DCVs bearing syt I or syt IV have more kiss-and-run events (37.2 ± 6.3% and 42.8 ± 5.9%, respectively), DCVs bearing syt VII have few (6.9 ± 3.0%), and DCVs bearing syt IX have an intermediate fraction (15.5 ± 8.0%; Figure 4G). These results indicate that the DCVs targeted by different syt isoforms have different preferential modes of exocytosis.

Plotting the percentage of kiss-and-run events against DCV diameter from immunogold electron microscopy (Figure 1) showed a strong inverse correlation between release mode and DCV size for the syt isoforms that stimulate fusion but not for the inhibitory isoform syt IV (Figure 4K). The fast decay times for the different isoforms showed small but statistically significant differences (Figure 4L), increasing in the order syt I, syt IX, syt VII. This sequence matches that of DCV size from electron microscopy and indicates that reacidification of larger vesicles requires more time. However, the syt isoform could also influence the kinetics of fusion pore closure (Wang *et al.*, 2003; Zhang *et al.*, 2009a). By contrast, the slow decay time for syt VII–pHluorin was about three times longer than for the other isoforms (Figure 4L), and this must reflect either a lower lateral diffusion coefficient or anchoring to other structures in either the membrane or cytoplasm. The much greater fraction of persistent events with syt VII–pHluorin (Figure 4J) could indicate that this isoform is more likely to form clusters (Willig *et al.*, 2006), in keeping with its strong tendency to homo-oligomerize (Fukuda and Mikoshiba, 2000). However, syt I–pHluorin does not cluster as much as native syt I (Opazo *et al.*, 2010).

As already noted, syt IV differs from the other syt isoforms of PC12 cells in being a negative regulator of exocytosis (Wang *et al.*, 2001). Indeed, in TIRF experiments syt IV-pHluorin–bearing DCVs exhibited a significantly lower secretion rate (Figure 4M) and had a higher percentage of kiss-and-run events than the other isoforms (Figure 4J), confirming previous results obtained with amperometry (Wang *et al.*, 2003). In the plot of kiss-and-run percentage versus DCV size, the syt IV point falls far off the fitted line for the exocytosis stimulating syt isoforms in Figure 5D, suggesting a different role for syt IV in the regulation of exocytosis. The decay time of kiss-and-run events in syt IV–bearing DCVs was slower than in syt I–bearing DCVs, whereas the decay time of full-fusion events was the same (Figure 4L).

Release mode of syt I–bearing DCVs

We further explored the possibility that DCVs harbor multiple syt isoforms by conducting experiments in which different molecules were used to trigger and to report exocytosis. Using syt I–pHluorin as the reporter, we therefore performed TIRF microscopy experiments and targeted different syt isoforms for activation using different divalent cations. The divalent cation selectivity of syt isoforms suggests the division of syt I–bearing DCVs into three groups. Ba^{2+} defines a group of syt I–bearing DCVs in which syt VII mediates exocytosis. Sr^{2+} defines a group of syt I–bearing DCVs in which the sensors are syt VII and syt IX. Ca^{2+} defines a group of syt I–bearing DCVs in which syt I, syt VII, and syt IX all trigger exocytosis. These groups are not mutually exclusive, and their overlaps are illustrated in Figure 5A. As in exocytosis of syt I-pHluorin–bearing vesicles triggered by Ca^{2+} (Figure 4D), two peaks were identified in the decay time distribution of exocytosis triggered by either Sr^{2+} (Figure 5B) or Ba^{2+} (Figure 5C). Exocytosis triggered by Ca^{2+} had the greatest preference for kiss-and-run, exocytosis triggered by Ba^{2+} had the weakest, and exocytosis triggered by Sr^{2+} was intermediate (Figure 5D). Kiss-and-run events triggered by Ba^{2+} decayed significantly more slowly than those triggered by either Ca^{2+} or Sr^{2+} (Figure 5E), which can be explained by the fact that the DCVs bearing Ba^{2+} are larger and reacidify more slowly (as in Figure 4L). Decay times for full fusion were not changed by different divalent cations (Figure 5E). Secretion rates were slowest for exocytosis triggered by Ba^{2+}, intermediate for exocytosis triggered by Sr^{2+}, and fastest for exocytosis triggered by Ca^{2+} (Figure 5F). This most likely reflects the number of DCVs with sensors for the corresponding divalent cation. syt VII is a low-abundance protein in PC12 cells (Tucker *et al.*, 2003; Wang *et al.*, 2005), and since Ba^{2+} targets this isoform it will trigger the fusion of the fewest DCVs. These results demonstrated that syt I–bearing DCVs can be directed to undergo different modes of exocytosis by engaging different syt isoforms as sensors.

Differential syt IV effects on DCVs bearing positive regulators

Amperometry recording has shown that syt IV slows exocytosis and favors kiss-and-run (Wang *et al.*, 2001, 2003), and the present study confirmed that result using TIRF (Figure 4M). syt IV does not bind Ca^{2+} (Dai *et al.*, 2004), and its inhibitory action probably depends on interactions with other syt isoforms or syt-binding partners. We therefore examined the effect of elevated syt IV levels on syt I–, VII–, and IX–mediated liposome fusion in vitro (Bhalla *et al.*, 2008). syt IV inhibited liposome fusion in the presence of each of the three other syt isoforms to the same degree (Figure 6, A–D) but with different efficacies. syt VII–mediated liposome fusion was inhibited with the highest efficacy ($[\text{syt IV}]_{½}$ = 1.12 μM), syt IX–mediated liposome fusion with an intermediate efficacy ($[\text{syt IV}]_{½}$ = 2.26 μM), and syt I–mediated liposome fusion with the lowest efficacy ($[\text{syt IV}]_{½}$ = 4.63 μM) (Figure 6D). Thus the inhibitory efficacy of syt IV depends on which Ca^{2+} sensor is selected.

Turning to PC12 cells, we added forskolin to the culture medium to elevate syt IV levels (Ferguson *et al.*, 1999; Wang *et al.*, 2003). Amperometry studies showed that forskolin and syt IV overexpression alter the kinetics of exocytosis from PC12 cells in similar ways (Ferguson *et al.*, 1999; Wang *et al.*, 2003). The decay time distribution for syt I–pHluorin showed two peaks, but the fast peak corresponding to kiss-and-run was more prominent (Figure 7A). By contrast, the induction of syt IV left the distribution of decay times for syt VII–pHluorin essentially unchanged (Figure 7B) compared with the control (Figure 4E). It was not possible to obtain a distribution with syt IX–pHluorin because the secretion rate measured with this probe in forskolin-treated cells was too low. syt IV induction with forskolin reduced the rate of secretion measured with syt I–pHluorin nearly threefold (Figure 7C), almost eliminated secretion measured with syt IX–pHluorin (Figure 7D), and had no discernible effect on secretion measured with syt VII–pHluorin (Figure 7E). After syt IV induction, syt I–bearing DCVs showed a greater preference for kiss-and-run (Figure 7F) and a significantly longer kiss-and-run decay time, but the full-fusion decay time remained unaltered (Figure 7H). In view of our in vitro results with syt VII (Figure 6B), it was surprising that syt IV induction did not significantly alter the release of syt VII DCVs; the secretion rate, kiss-and-run preference, and decay times

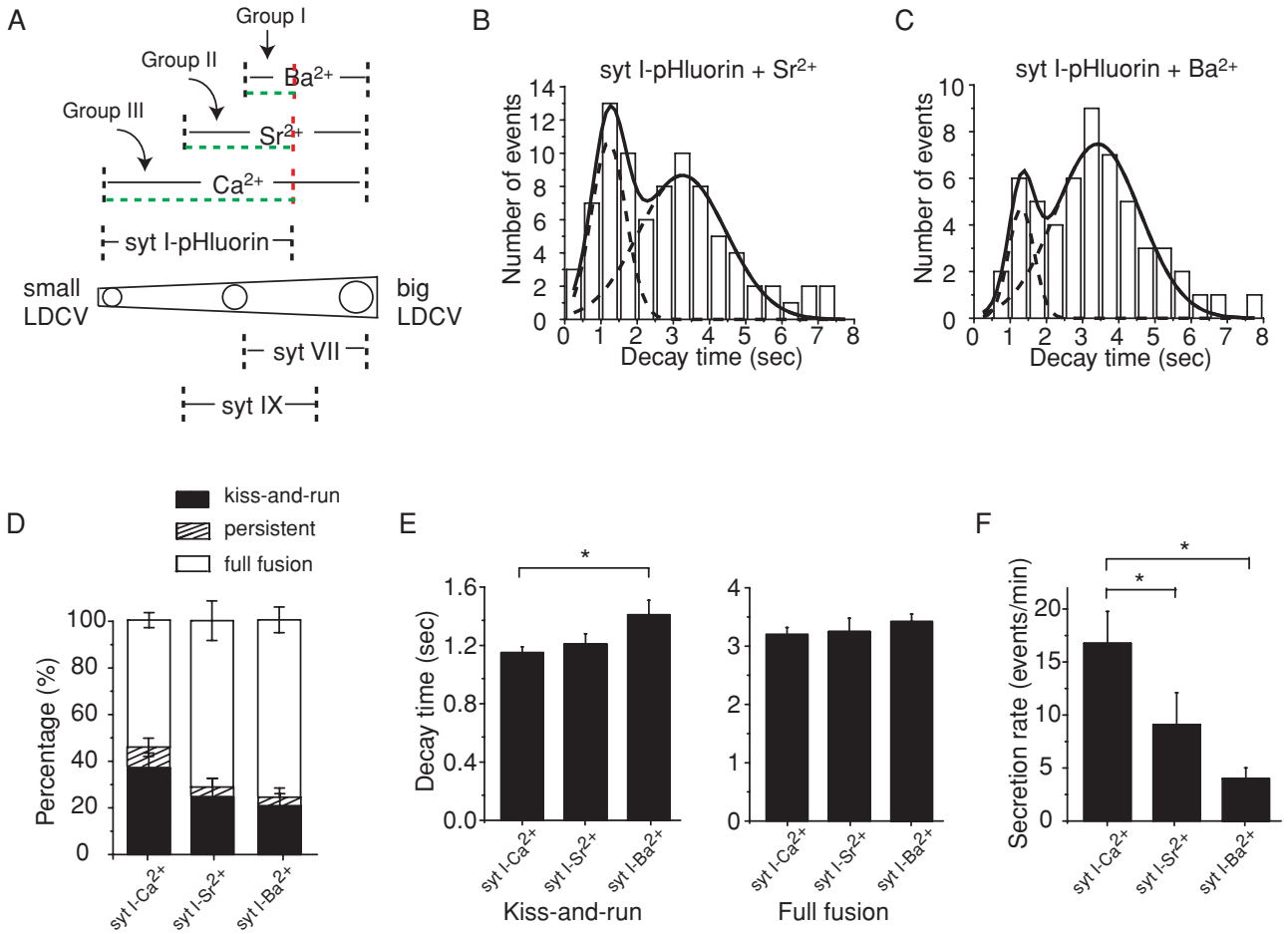

FIGURE 5: Different release modes in syt I-bearing DCVs. (A) A size diagram for DCV exocytosis triggered by different divalent cations. Distributions of TIRF decay times of syt I-pHluorin–transfected cells were plotted for release triggered by Sr^{2+} (B) and Ba^{2+} (C) (note that the corresponding plot for Ca^{2+} is shown in Figure 4D). Distributions showed two peaks with different areas. Percent of events that are kiss-and-run (D), rapid and slow decay times (E), and secretion rate (F) for exocytosis triggered by Ca^{2+}, Sr^{2+}, and Ba^{2+}, using syt I–pHluorin signals. From 56 to 131 events were used for decay time analysis and 56–218 events for secretion rate analysis for recordings from 8–14 cells for each divalent cation. Error bars represent SEM. *$p < 0.05$.

of kiss-and-run and full-fusion events remained the same (Figure 7, E, G, and I). The interaction between syt VII and other molecules in the cellular assay might overcome the inhibition of fusion by syt IV, and this could account for the discrepancy between the in vitro results and the results from PC12 cells. Collectively, syt IV strongly inhibited exocytosis of syt I–bearing or syt IX–bearing DCVs, shifted the mode of syt I–bearing DCVs to kiss-and-run, and had little if any effect on exocytosis of syt VII–bearing DCVs.

DISCUSSION

This study explored the heterogeneity of DCVs in PC12 cells at both the molecular and functional levels. Different-sized DCVs harbor different syt isoforms, and these isoforms confer functional differences in the ease of triggering fusion, the mode of exocytosis, and sensitivity to inhibition by syt IV. Small DCVs harbor more syt I and prefer kiss-and-run. Large DCVs harbor more syt VII and prefer full fusion. Intermediate-sized DCVs harbor more syt IX and are also intermediate in their preference for kiss-and-run versus full fusion. syt IV induction inhibits the fusion of syt IX–bearing vesicles strongly, syt I–bearing vesicles moderately, and syt VII–bearing vesicles hardly at all. If different secreted substances cosort with syt isoforms or are packaged in DCVs with different sizes, then the various functional differences reported here can provide a mechanism for selective secretion. Furthermore, by favoring full fusion or kiss-and-run the targeting of syt isoforms would direct the selective release of either only small molecules or both small and large molecules from the same vesicle. By activating different syt isoforms, different levels of Ca^{2+} will promote kiss-and-run or full fusion and thus control the selectivity of secretion.

Our immunogold labeling experiments indicated a considerable degree of segregation of the syt isoforms, with ~50% of the DCVs lacking each one. However, with each of these isoforms present on ~50% of the DCVs, it is likely that the DCV populations harboring each isoform show some overlap and that DCVs harbor multiple syt isoforms. syt I and syt IV labeling of individual DCVs in PC12 cells has been reported previously (Wang *et al.*, 2003; Zhu *et al.*, 2007), as has partial colocalization of syt I and syt VII (Martinez *et al.*, 2000; Wang *et al.*, 2005). Our immunofluorescence results support some segregation of syt I and syt VII to different compartments, but syt I, IV, and IX have indistinguishable distributions within cells (Figure 3). Our functional experiments in which Ba^{2+}/Sr^{2+} triggered fusion of syt I-pHfluorin–bearing DCVs (Figure 5) makes a stronger case for the

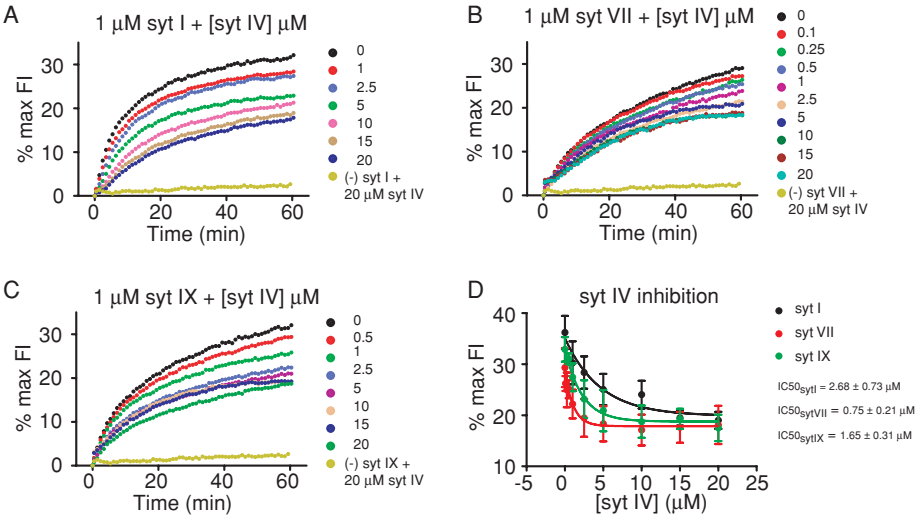

FIGURE 6: The effect of syt IV on fusion in liposomes bearing distinct syt isoforms. (A–C) syt IV inhibited syt I–, syt VII–, and syt IX–mediated liposome fusion in vitro. (D) The dependence of inhibition of fusion on syt IV concentration. At least four independent experiments were performed for in vitro fusion assays.

presence of syt I on vesicles that also harbor syt VII and syt IX. Thus the segregation of syt isoforms to different DCV populations is partial. A simple explanation for these results is syt isoform sorting to DCVs based on size, with overlap in size preference. Targeting mechanisms based on molecular recognition are also possible. The collection of syt isoforms on a DCV represents an important defining feature with clear functional consequences. Thus the combinatorics of syt isoform distribution on DCVs deserves further study, as does the relation between syt isoform sorting and content sorting.

The distinct Ca^{2+} sensitivities of syt isoforms (Bhalla *et al.*, 2005; Hui *et al.*, 2005) emerges as a critical property in determining the functional significance of sorting to different DCVs. syt VII has a high Ca^{2+} sensitivity, syt IX an intermediate Ca^{2+} sensitivity, and syt I a low Ca^{2+} sensitivity. syt isoforms also influence the mode of exocytosis in PC12 cells (Wang *et al.*, 2003; Zhu *et al.*, 2007) as well as in neurons (C. Dean, F. M. Dunning, H. Liu H, and E. R. Chapman, unpublished data), and the present results indicate that syt I shows the strongest preference for kiss-and-run, syt IX shows an intermediate preference, and syt VII strongly favors full fusion. It is notable that a recent analysis of amperometry prespike feet indicated that syt VII shows a slightly greater tendency for kiss-and-run (Zhang *et al.*, 2010a). However, TIRF microscopy almost certainly detects longer-lived kiss-and-run events than those related to prespike feet, so that comparisons between the two approaches are difficult. Similar disparities have been noted between the effects of syt IV on events recorded with amperometry and capacitance (Zhang *et al.*, 2010b). It is hoped that careful comparative studies in the same system will clarify the relation among exocytosis measurements with TIRF, amperometry, and capacitance. In PC12 cells overexpressing syt I, high concentrations of Ca^{2+} favor fusion pore openings resolving to spikes, and presumably full fusion (Wang *et al.*, 2006). Low concentrations of Ca^{2+} will activate exocytosis of the high-affinity sensor syt VII, and this isoform displays a strong preference for full fusion. Higher concentrations of Ca^{2+} will then activate syt IX, and further increases will activate syt I. These less sensitive isoforms favor kiss-and-run more strongly. Thus DCVs bearing syt isoforms with different Ca^{2+} sensitivities and different preferred release modes can effect a graded transition in release mode with increasing Ca^{2+} concentration. The activation of these different Ca^{2+} sensors by stimuli that produce low or high cytoplasmic Ca^{2+} concentrations offers a molecular mechanism for the shifts in release mode in endocrine cells as stimulus strength increases (Fulop *et al.*, 2005; MacDonald *et al.*, 2006).

Neuropeptides generated by the same cell may be packaged into distinct DCVs (Fisher *et al.*, 1988; Sossin *et al.*, 1990; Glombik and Gerdes, 2000) and secreted preferentially depending on the form of stimulation (Childs *et al.*, 1987; Perello *et al.*, 2008). Even when neuropeptides are packaged into the same DCVs their ratios can vary (Salio *et al.*, 2006). The amino acid sequences for sorting membrane proteins into endoplasmic reticulum, lysosomes, and some other compartments are well known (Sossin and Scheller, 1991), but the amino acid sequences directing membrane proteins to DCVs have not yet been determined (Glombik and Gerdes, 2000). The targeting of proteins to different-sized DCVs could imply the existence of a size signal in the sorting machinery. However, DCV maturation entails a reduction in size (Kim *et al.*, 2006), and regulation at these later stages could contribute to DCV heterogeneity in both size and composition. Membrane proteins can be selectively sorted to DCVs via interaction with stored neuropeptides (Guan *et al.*, 2005). This raises an important question about whether neuropeptides and proteins that regulate DCV content interact with syt isoforms and whether these interactions contribute to coordinated sorting of syt isoforms and content to DCVs with distinct sizes.

Kiss-and-run and vesicle recycling are very different in SVs and DCVs. Recycled SVs refill by an uptake process, but neuropeptides must be packaged into DCVs during their genesis from the *trans*-Golgi network. Thus neuropeptides cannot be secreted from recycled DCVs immediately after full fusion. By contrast, vesicular monoamine transporters make it possible to reload recycled DCVs. Because biogenic amines can escape through metastable fusion pores during kiss-and-run (Alvarez de Toledo *et al.*, 1993; Zhou *et al.*, 1996; Wang *et al.*, 2003), reloading of these vesicles would be an important step in recycling and restoring function. The selective release and refilling of amines through kiss-and-run would allow repeated use of a DCV for one form of release while retaining neuropeptides for release triggered by a stronger stimulus.

syt IV is unusual among the members of the syt protein family in its lack of Ca^{2+} binding (Dai *et al.*, 2004) and its inhibition of exocytosis (Wang *et al.*, 2001; Dean *et al.*, 2009). This early-immediate gene product (Vician *et al.*, 1995) is abundant in peptidergic nerve terminals (Zhang *et al.*, 2009a) and is induced by electrical activity (Vician *et al.*, 1995; Ibata *et al.*, 2000; Dean *et al.*, 2009), drugs of abuse (Denovan-Wright *et al.*, 1998; Peng *et al.*, 2002), and behavioral transitions (Poopatanapong *et al.*, 2006). syt IV had no effect on exocytosis of syt VII DCVs but almost completely shut down the exocytosis of syt IX–bearing DCVs (Figure 7). These results suggest that syt IV targets specific populations of DCVs for inhibition. This represents another functional distinction between populations of DCVs with different sizes and syt isoforms. These results suggest that the induction of syt IV will not reduce DCV exocytosis globally but will show selectivity in the inhibition of some DCVs but not others. This will allow syt IV to influence behaviors in more complex ways and to

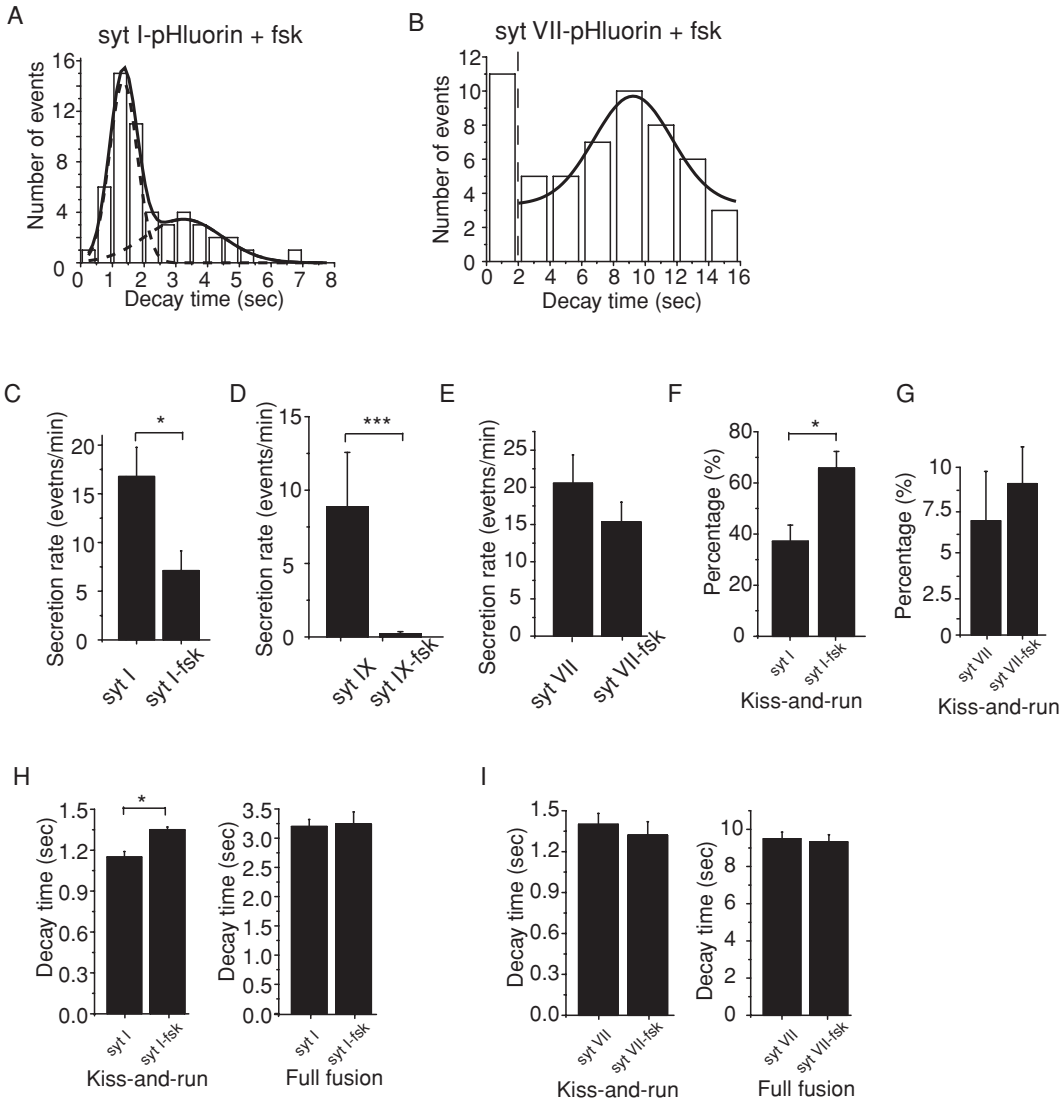

FIGURE 7: The effect of syt IV induction on exocytosis. Cells were treated with forskolin to induce syt IV and transfected with syt–pHluorin constructs so that exocytosis could be studied with TIRF. (A) syt I–pHluorin events decayed with varying rates, and the decay time distribution revealed two peaks corresponding to kiss-and-run and full fusion (compare with Figure 4D). (B) syt VII–pHluorin events had a decay time distribution similar to that in syt VII-pHluorin–transfected cells without forskolin treatment (Figure 4E). Forskolin treatment reduced the secretion rate of syt I-pHluorin–bearing DCVs (C) and syt IX-pHluorin–bearing DCVs (D) but not syt VII–bearing DCVs (E). Forskolin increased the percentage of syt I–pHluorin events that were kiss-and-run (F) but had no significant effect on the kiss-and-run percentage with syt VII–bearing DCVs (G). (H) Forskolin treatment induced a small but statistically significant increase in the fast decay time of syt I–pHluorin events but produced no change in the slow decay time. (I) Forskolin treatment failed to alter the percentage of kiss-and-run events or decay times of syt VII–bearing vesicles. From 78 to 131 events were used for decay time analysis and 3–262 events for secretion rate analysis for recordings from 8–19 cells. Error bars represent SEM. *$p < 0.05$; ***$p < 0.001$.

coordinate the activity of systems dependent upon multiple chemical signals.

This work has demonstrated important functional distinctions in how three syt isoforms regulate Ca^{2+}-triggered exocytosis. syt I, syt VII, and syt IX differ in their Ca^{2+} sensitivity, their divalent cation sensitivity, their preference for kiss-and-run over full fusion, and their sensitivity to inhibition by the induction of syt IV. Different-sized DCVs with different proportions of these proteins will undergo exocytosis in response to different forms of stimulation. These results thus indicate that members of the syt protein family provide the functional diversity for multiple levels of control in the selective release of different substances packaged either in the same DCV or different DCVs.

MATERIALS AND METHODS

Plasmid construction

The syt I–pHluorin construct (Miesenbock *et al.*, 1998) was provided by Tim Ryan. From this construct we generated syt IV–pHluorin, syt VII–pHluorin, and syt IX–pHluorin, and we cloned them into pCI vector (Promega, Madison, WI). syt I C2AB, syt VII C2AB, and syt IX C2AB were expressed in the pTrcHisA vector (Invitrogen, Carlsbad, CA). syt IV C2AB was cloned into the pET vector (Invitrogen). Full-length syt VII was also cloned into the pCMV-Myc vector (Clontech, Mountain View, CA). Plasmids encoding SNAP-25, syntaxin 1a, and synaptobrevin were provided by J. E. Rothman (Yale University, New Haven, CT). All constructs were verified by sequencing.

Protein expression and purification

For His-tagged syt I C2AB, syt IV C2AB, syt VII C2AB, and syt IX C2AB, *Escherichia coli* was grown at 37°C to an OD_{600} of 0.8 and treated with 0.4 mM isopropyl β-D-1-thiogalactopyranoside to induce protein expression. Four hours after induction the bacteria were collected by centrifugation, resuspended in His_6 buffer (25 mM HEPES-KOH, 500 mM NaCl, 20 mM imidazole), and sonicated (two times, 45 s; 50% duty cycle). Triton X-100 (2%) and protease inhibitors (1 μg/ml aprotinin, pepstatin, and leupeptin; 0.5 mM phenylmethylsulfonyl fluoride) were added to the sonicated material and incubated for 2–3 h with rotation at 4°C. Samples were centrifuged to remove the insoluble material, and the supernatant was incubated with Ni^{2+}-Sepharose HP beads (GE-Amersham Biosciences, Piscataway, NJ) overnight. The following day, the Ni^{2+} beads were washed twice with His_6 wash buffer containing 25 mM HEPES, 1 M NaCl, 1 mM $MgCl_2$, 20 mM imidazole, and 0.1 mg/ml RNase and DNase. Beads were collected and eluted with 1.5 volumes of elution buffer (25 mM HEPES-KOH, 400 mM KCl, 500 mM imidazole, 5 mM 2-mercaptoethanol). Eluted protein was dialyzed against a solution containing 25 mM HEPES-KOH, 250 mM KCl, 10% glycerol, and 0.16 g/l dithiothreitol (DTT).

For his-tagged t-SNARE heterodimers (syntaxin and SNAP-25) and the v-SNARE synaptobrevin, *E. coli* were grown and collected as described previously. The pellet was resuspended in resuspension buffer (25 mM HEPES-KOH, 400 mM KCl, 20 mM imidazole, and 5 mM 2-mercaptoethanol), sonicated, and treated with Triton X-100 (2%), protease inhibitors, RNase, and DNase. Insoluble material was removed by centrifugation, and the supernatant was applied to a Ni^{2+} column using AKTA FPLC (GE-Amersham Biosciences). The column was washed extensively with resuspension buffer containing 1% Triton X-100 and then *n*-octylglucoside wash buffer (25 mM HEPES-KOH, 400 mM KCl, 50 mM imidazole, 10% glycerol, 5 mM 2-mercaptoethanol, and 1% *n*-octylglucoside). The bound protein was eluted using *n*-octylglucoside wash buffer with 500 mM imidazole.

All proteins were subjected to SDS–PAGE and stained with Coomassie blue to determine concentration against a bovine serum albumin standard curve.

Protein reconstitution

Liposomes with t-SNAREs or v-SNARE were prepared as described previously (Tucker *et al.*, 2004). Briefly, lipid mixtures (t-SNARE vesicles: 15% PS, 30% PC, 55% PC; v-SNARE vesicles: 15% PS, 27% PE, 55% PC, 1.5% NBD-PE, 1.5% rhodamine-PE) (Avanti Polar Lipids, Alabaster, AL) in chloroform were dried under a stream of nitrogen and subjected to vacuum for >1 h. The syntaxin·SNAP-25 complex was diluted to 0.8 mg/ml, and synaptobrevin was diluted to 0.19 mg/ml. The dried lipid was suspended in the respective protein solutions and diluted with reconstitution buffer (25 mM HEPES-KOH, 100 mM KCl, 10% glycerol, 1 mM DTT). Vesicles were dialyzed against reconstitution buffer overnight, collected, mixed with 80% Accudenz, and transferred into ultra clear centrifuge tubes. A step gradient was prepared by the addition of 30 and 0% Accudenz layers onto the vesicle layer. The samples were centrifuged at 55,000 rpm for 2 h (SW55 rotor; Beckman Coulter, Brea, CA), and vesicles were collected from the 0/30% interface and analyzed by SDS–PAGE to verify protein incorporation.

Fusion assays and data analysis

Scaled-down liposome fusion assays were carried out in white-bottom 96-well plates with total reaction volumes of 75 μl. Each reaction contained 4.5 μl of t-SNARE vesicles or protein-free vesicles, 0.5 μl of NBD-rhodamine–labeled v-SNARE vesicles, and 1.5 μl of 10 mM ethylene glycol tetraacetic acid. Purified proteins were added to each reaction as designated. Samples were preincubated at 37°C for 20 min, followed by addition of designated concentrations of Ca^{2+}, Sr^{2+}, or Ba^{2+}. Following divalent cation addition fluorescence intensity was monitored for 60 min at 37°C using a Synergy HT plate reader (BioTek, Winooski, VT) equipped with 460/40 excitation and 530/25 emission filters. The maximum fluorescence signal was obtained by addition of 25 μl of *n*-dodecyl β-D-maltoside to each reaction well; samples were monitored for an additional 30 min until a stable signal was obtained. Fusion data were normalized by setting the initial time point to 0% and the maximal fluorescence signal in detergent to 100%.

Amperometry and data analysis

PC12 cells were cultured in an incubator at 37°C in 10% CO_2/air, split into 10-mm dishes coated with collagen I (BD Biosciences, San Jose, CA) and poly-D-lysine (Sigma-Aldrich, St. Louis, MO), and loaded with 1.5 mM norepinephrine and 0.5 mM ascorbate 14–16 h before experiments. Amperometry was performed 48–96 h after transfection.

Norepinephrine release was recorded with a VA-10 amperometry amplifier (ALA Scientific, Farmingdale, NY) using 5-μm carbon fiber electrodes held at 650 mV (Zhang and Jackson, 2008). Cells were bathed in a solution containing 150 mM NaCl, 4.2 mM KCl, 1 mM NaH_2PO_4, 0.7 mM $MgCl_2$, 2 mM $CaCl_2$, and 10 mM HEPES, pH 7.4. Secretion was evoked by pressure application of a solution identical to bathing solution but with 105 mM KCl and 5 mM NaCl.

Amperometry spikes were analyzed as described previously (Zhang and Jackson, 2008). Spikes with peak amplitudes >2 pA were counted for secretion rate. Fusion pore lifetimes were taken as the duration of prespike feet measured for spikes with amplitudes >20 pA. Student's *t* test was used to evaluate statistical significance.

Immunogold electron microscopy

PC12 cells transfected with syt isoform-pHluorin–encoding DNA were sectioned at 100 nm and fixed in 4% paraformaldehyde/0.1% glutaraldehyde in 0.1 M sodium phosphate buffer (PB), pH 7.4, at room temperature (RT) for 2 h. The fixed samples were rinsed five times for 5 min in PB at room temperature and cryoprotected in 10%, then 20% glycerin in PB for 1 h (RT), and finally 30% glycerin overnight at 4°C. The fixed and cryoprotected samples were rapidly frozen in liquid propane at −180°C using a plunge freezer (Reichert-Jung KF80; Riechert, Vienna, Austria) and transferred to methanol containing 0.5% uranyl acetate at −90°C for 48 h for freeze substitution (Leica EM AFS; Leica Microsystems, Buffalo Grove, IL). At the end of the 48-h substitution, samples were slowly warmed to −45°C (for 9 h, 5°C/h). Next the samples were rinsed, infiltrated, and embedded in HM20 Lowicryl resin (Polysciences, Warrington, PA). All the following steps were performed at −45 °C. Samples were rinsed in pure methanol for 0.5 h, HM20:methanol (1:1) for 2 h, HM20:methanol (1.5:1) for 2 h, and pure HM20 for 2 h, and polymerized under UV light for 48 h. Following initial polymerization, the samples were warmed gradually (10°C/h) for 6.5 h to 20°C and further polymerized for 48 h. Polymerized samples were sectioned on a Leica UC6 ultramicrotome and sections collected on Pioloform-coated Ni grids. Immunolabeling was performed with anti-GFP primary antibody (Abcam, Cambridge, MA) and 10 nm of colloidal gold goat anti–mouse secondary antibody. Immunolabeled sections were post stained in lead citrate and uranyl acetate and viewed on a Philips CM120 electron microscope. Images were collected with a

Soft Imaging Systems MegaView III digital camera (Olympus Soft Imaging Solutions, Singapore). Dense-core vesicles were recognized by the dense core, and those labeled with gold particles were selected for further analysis. Because the vesicles that were analyzed were not near the *trans*-Golgi network, we consider the majority of them to be mature. Membranes around the cores were visible and diameters were measured with the computer program ImageJ (National Institutes of Health, Bethesda, MD). Statistic significance between groups was determined by Student's *t* test.

Immunocytochemistry

PC12 cells were plated on poly-D-lysine– and collagen-coated coverslips at approximately the same density for each labeling condition. Due to low expression levels of syt IV, we used forskolin (fsk) to induce syt IV overexpression (Wang *et al.*, 2003). Endogenous syt VII was also expressed at low levels, so we overexpressed c-myc–syt VII by transfection of PC12 cells. Cells were washed twice in phosphate-buffered saline (PBS) without Ca^{2+} or Mg^{2+} and fixed for 15 min in 4% paraformaldehyde in PBS. Cells were washed twice in PBS, permeabilized with 0.1% Triton X-100 for 10 min, and blocked for 1 h with blocking buffer consisting of 10% goat serum. Primary and secondary antibodies were diluted in blocking buffer. Cells were incubated overnight with a combination of the following primary antibodies: monoclonal anti–syt I antibody (antibody 41.1), polyclonal anti–syt I antibody (Synaptic Systems, Göttingen, Germany), monoclonal and polyclonal anti–syt IX antibodies (prepared in house, with specificity demonstrated by Western blot analysis of each of the relevant recombinant isoforms; unpublished data), monoclonal and polyclonal anti–c-myc antibodies (Abcam), polyclonal anti–syt IV antibody (Synaptic Systems), monoclonal anti–chromogranin B antibody (BD Bioscience), and monoclonal anti–syntaxin 1A antibody (HPC-1). The cells were then washed four times in PBS and incubated for 1 h with Alexa-conjugated anti-rabbit and anti-mouse secondary antibodies (Molecular Probes/Invitrogen, Eugene, OR). After five 10-min washes in PBS, coverslips were mounted on slides with Prolong mounting reagent (Molecular Probes/Invitrogen). Imaging and analysis followed previous methods (Wang *et al.*, 2005). Cells were imaged on a Nikon TE300 inverted microscope using a 100×, 1.4–numerical aperture (NA) objective lens. Images were acquired using a Princeton Instruments Micromax cooled charge-coupled device camera (Roper Scientific, Princeton, NJ) controlled by Metamorph software (Universal Imaging Corp, West Chester, PA). Colocalization was quantified by thresholding the green and red images and by measuring Mander's overlap coefficient red to green and green to red in each optical section. Analysis was performed with ImageJ and the JaCoP plug-in (Bolte and Cordelieres, 2006). Pooled data are expressed as mean ± SEM.

Total internal reflection fluorescence microscopy

PC12 cells were split onto 35-mm coverslips (MatTek, Ashland, MA) in six-well plates coated with collagen I (BD Biosciences) and poly-D-lysine (Sigma-Aldrich) and transfected using Lipofectamine 2000 (Invitrogen). Images of exocytosis were acquired in an incubation buffer (150 mM NaCl, 4.2 mM KCl, 1 mM NaH_2PO_4, 0.7 mM $MgCl_2$, 2 mM $CaCl_2$, and 10 mM HEPES, pH 7.4) or depolarization buffer (same as incubation buffer with 95 mM NaCl and 56 mM KCl) using an IX81-ZDC microscope (Olympus, Center Valley, PA) configured for evanescent field excitation and equipped with a 1.42-NA objective (APO 100× and APO 60×; Olympus) controlled with SlideBook 5.0 software (Olympus Workstation). Illumination at 488 nm was provided by an argon ion laser (IMA 100; CVI Melles Griot, Albuquerque, NM). TIRF images were recorded at 100-ms intervals for 50 s and analyzed using SlideBook 5.0 software (Olympus Workstation), Origin (OriginLab, Northampton, MA), and ImageJ 1.42. All fluorescence values were corrected by subtracting background. The penetration depth of the evanescent field was ~70 nm.

ACKNOWLEDGMENTS

This work was supported by National Institutes of Health Grant NS44057 to M.B.J. E.R.C. is a Howard Hughes Medical Institute Investigator. We thank R. Massey and B. August for assistance with electron microscopy. We thank Camin Dean, Sam Kwon, and Felix Yeh for helpful discussions and comments.

REFERENCES

Ahras M, Otto GP, Tooze SA (2006). Synaptotagmin IV is necessary for the maturation of secretory granules in PC12 cells. J Cell Biol 173, 241–251.

Alvarez de Toledo G, Fernandez-Chacon R, Fernandez JM (1993). Release of secretory products during transient vesicle fusion. Nature 363, 554–558.

Ariga T, Macala LJ, Saito M, Margolis RK, Greene LA, Margolis RU, Yu RK (1988). Lipid composition of PC12 pheochromocytoma cells: characterization of globoside as a major neutral glycolipid. Biochemistry 27, 52–58.

Atluri PP, Ryan TA (2006). The kinetics of synaptic vesicle reacidification at hippocampal nerve terminals. J Neurosci 26, 2313–2320.

Augustine GJ (2001). How does calcium trigger neurotransmitter release? Curr Opin Neurobiol 11, 320–326.

Bean AJ, Zhang X, Hokfelt T (1994). Peptide secretion: what do we know? FASEB J 8, 630–638.

Bhalla A, Chicka MC, Chapman ER (2008). Analysis of the synaptotagmin family during reconstituted membrane fusion. Uncovering a class of inhibitory isoforms. J Biol Chem 283, 21799–21807.

Bhalla A, Tucker WC, Chapman ER (2005). Synaptotagmin isoforms couple distinct ranges of Ca^{2+}, Ba^{2+}, and Sr^{2+} concentration to SNARE-mediated membrane fusion. Mol Biol Cell 16, 4755–4764.

Bolte S, Cordelieres FP (2006). A guided tour into subcellular colocalization analysis in light microscopy. J Microsc 224, 213–232.

Bowser DN, Khakh BS (2007). Two forms of single-vesicle astrocyte exocytosis imaged with total internal reflection fluorescence microscopy. Proc Natl Acad Sci USA 104, 4212–4217.

Chapman ER (2008). How does synaptotagmin trigger neurotransmitter release? Annu Rev Biochem 77, 615–641.

Childs GV, Unabia G, Tibolt R, Lloyd JM (1987). Cytological factors that support nonparallel secretion of luteinizing hormone and follicle-stimulating hormone during the estrous cycle. Endocrinology 121, 1801–1813.

Craxton M (2007). Evolutionary genomics of plant genes encoding N-terminal-TM-C2 domain proteins and the similar FAM62 genes and synaptotagmin genes of metazoans. BMC Genomics 8, 259.

Dai H, Shin OH, Machius M, Tomchick DR, Sudhof TC, Rizo J (2004). Structural basis for the evolutionary inactivation of Ca^{2+} binding to synaptotagmin 4. Nat Struct Mol Biol 11, 844–849.

Dean C, Liu H, Dunning FM, Chang PY, Jackson MB, Chapman ER (2009). Synaptotagmin-IV modulates synaptic function and long-term potentiation by regulating BDNF release. Nat Neurosci 12, 767–776.

Denovan-Wright EM, Newton RA, Armstrong JN, Babity JM, Robertson HA (1998). Acute administration of cocaine, but not amphetamine, increases the level of synaptotagmin IV mRNA in the dorsal striatum of rat. Brain Res Mol Brain Res 55, 350–354.

Ferguson GD, Thomas DM, Elferink LA, Herschman HR (1999). Synthesis degradation, and subcellular localization of synaptotagmin IV, a neuronal immediate early gene product. J Neurochem 72, 1821–1831.

Fisher JM, Sossin W, Newcomb R, Scheller RH (1988). Multiple neuropeptides derived from a common precursor are differentially packaged and transported. Cell 54, 813–822.

Fukuda M, Kanno E, Satoh M, Saegusa C, Yamamoto A (2004). Synaptotagmin VII is targeted to dense-core vesicles and regulates their Ca^{2+}-dependent exocytosis in PC12 cells. J Biol Chem 279, 52677–52684.

Fukuda M, Kowalchyk JA, Zhang X, Martin TF, Mikoshiba K (2002). Synaptotagmin IX regulates Ca^{2+}-dependent secretion in PC12 cells. J Biol Chem 277, 4601–4604.

Fukuda M, Mikoshiba K (2000). Distinct self-oligomerization activities of synaptotagmin familyUnique calcium-dependent oligomerization properties of synaptotagmin VII. J Biol Chem 275, 28180–28185.

Fulop T, Radabaugh S, Smith C (2005). Activity-dependent differential transmitter release in mouse adrenal chromaffin cells. J Neurosci 25, 7324–7332.
Gaffaney JD, Dunning FM, Wang Z, Hui E, Chapman ER (2008). Synaptotagmin C2B domain regulates Ca^{2+}-triggered fusion in vitro: critical residues revealed by scanning alanine mutagenesis. J Biol Chem 283, 31763–31775.
Gandhi SP, Stevens CF (2003). Three modes of synaptic vesicular recycling revealed by single-vesicle imaging. Nature 423, 607–613.
Glombik MM, Gerdes HH (2000). Signal-mediated sorting of neuropeptides and prohormones: secretory granule biogenesis revisited. Biochimie 82, 315–326.
Gong LW, Hafez I, Alvarez de Toledo G, Lindau M (2003). Secretory vesicles membrane area is regulated in tandem with quantal size in chromaffin cells. J Neurosci 23, 7917–7921.
Guan JS *et al.* (2005). Interaction with vesicle luminal protachykinin regulates surface expression of delta-opioid receptors and opioid analgesia. Cell 122, 619–631.
Hokfelt T, Broberger C, Xu ZQ, Sergeyev V, Ubink R, Diez M (2000). Neuropeptides—an overview. Neuropharmacology 39, 1337–1356.
Hokfelt T, Zhang X, Wiesenfeld-Hallin Z (1994). Messenger plasticity in primary sensory neurons following axotomy and its functional implications. Trends Neurosci 17, 22–30.
Holroyd P, Lang T, Wenzel D, De Camilli P, Jahn R (2002). Imaging direct, dynamin-dependent recapture of fusing secretory granules on plasma membrane lawns from PC12 cells. Proc Natl Acad Sci USA 99, 16806–16811.
Hui E, Bai J, Wang P, Sugimori M, Llinas RR, Chapman ER (2005). Three distinct kinetic groupings of the synaptotagmin family: candidate sensors for rapid and delayed exocytosis. Proc Natl Acad Sci USA 102, 5210–5214.
Ibata K, Fukuda M, Hamada T, Kabayama H, Mikoshiba K (2000). Synaptotagmin IV is present at the Golgi and distal parts of neurites. J Neurochem 74, 518–526.
Kim T, Gondre-Lewis MC, Arnaoutova I, Loh YP (2006). Dense-core secretory granule biogenesis. Physiology (Bethesda) 21, 124–133.
Koh TW, Bellen HJ (2003). Synaptotagmin I, a Ca^{2+} sensor for neurotransmitter release. Trends Neurosci 26, 413–422.
MacDonald PE, Braun M, Galvanovskis J, Rorsman P (2006). Release of small transmitters through kiss-and-run fusion pores in rat pancreatic beta cells. Cell Metab 4, 283–290.
Marqueze B, Berton F, Seagar M (2000). Synaptotagmins in membrane traffic: which vesicles do the tagmins tag? Biochimie 82, 409–420.
Martinez I, Chakrabarti S, Hellevik T, Morehead J, Fowler K, Andrews NW (2000). Synaptotagmin VII regulates Ca(2+)-dependent exocytosis of lysosomes in fibroblasts. J Cell Biol 148, 1141–1149.
McNeilly AS, Crawford JL, Taragnat C, Nicol L, McNeilly JR (2003). The differential secretion of FSH and LH: regulation through genes, feedback and packaging. Reprod Suppl 61, 463–476.
Michael DJ, Geng X, Cawley NX, Loh YP, Rhodes CJ, Drain P, Chow RH (2004). Fluorescent cargo proteins in pancreatic beta-cells: design determines secretion kinetics at exocytosis. Biophys J 87, L03–05.
Miesenbock G, De Angelis DA, Rothman JE (1998). Visualizing secretion and synaptic transmission with pH-sensitive green fluorescent proteins. Nature 394, 192–195.
Opazo F, Punge A, Buckers J, Hoopmann P, Kastrup L, Hell SW, Rizzoli SO (2010). Limited intermixing of synaptic vesicle components upon vesicle recycling. Traffic 11, 800–812.
Peng W, Premkumar A, Mossner R, Fukuda M, Lesch KP, Simantov R (2002). Synaptotagmin I and IV are differentially regulated in the brain by the recreational drug 3,4-methylenedioxymethamphetamine (MDMA). Brain Res Mol Brain Res 108, 94–101.
Perello M, Stuart R, Nillni EA (2008). Prothyrotropin-releasing hormone targets its processing products to different vesicles of the secretory pathway. J Biol Chem 283, 19936–19947.
Poopatanapong A, Teramitsu I, Byun JS, Vician LJ, Herschman HR, White SA (2006). Singing, but not seizure, induces synaptotagmin IV in zebra finch song circuit nuclei. J Neurobiol 66, 1613–1629.
Salio C, Lossi L, Ferrini F, Merighi A (2006). Neuropeptides as synaptic transmitters. Cell Tissue Res 326, 583–598.
Shin OH, Rhee JS, Tang J, Sugita S, Rosenmund C, Sudhof TC (2003). Sr2+ binding to the Ca2+ binding site of the synaptotagmin 1 C2B domain triggers fast exocytosis without stimulating SNARE interactions. Neuron 37, 99–108.
Sossin WS, Fisher JM, Scheller RH (1990). Sorting within the regulated secretory pathway occurs in the trans-Golgi network. J Cell Biol 110, 1–12.
Sossin WS, Scheller RH (1991). Biosynthesis and sorting of neuropeptides. Curr Opin Neurobiol 1, 79–83.
Sudhof TC (2002). Synaptotagmins: why so many? J Biol Chem 277, 7629–7632.
Taraska JW, Almers W (2004). Bilayers merge even when exocytosis is transient. Proc Natl Acad Sci USA 101, 8780–8785.
Tsuboi T, Rutter GA (2003). Multiple forms of "kiss-and-run" exocytosis revealed by evanescent wave microscopy. Curr Biol 13, 563–567.
Tucker WC, Edwardson JM, Bai J, Kim HJ, Martin TF, Chapman ER (2003). Identification of synaptotagmin effectors via acute inhibition of secretion from cracked PC12 cells. J Cell Biol 162, 199–209.
Tucker WC, Weber T, Chapman ER (2004). Reconstitution of Ca2+-regulated membrane fusion by synaptotagmin and SNAREs. Science 304, 435–438.
Verhage M, McMahon HT, Ghijsen WE, Boomsma F, Scholten G, Wiegant VM, Nicholls DG (1991). Differential release of amino acids, neuropeptides, and catecholamines from isolated nerve terminals. Neuron 6, 517–524.
Vician L, Lim IK, Ferguson G, Tocco G, Baudry M, Herschman HR (1995). Synaptotagmin IV is an immediate early gene induced by depolarization in PC12 cells and in brain. Proc Natl Acad Sci USA 92, 2164–2168.
Wang CT, Bai J, Chang PY, Chapman ER, Jackson MB (2006). Synaptotagmin-Ca^{2+} triggers two sequential steps in regulated exocytosis in rat PC12 cells: fusion pore opening and fusion pore dilation. J Physiol 570, 295–307.
Wang CT, Grishanin R, Earles CA, Chang PY, Martin TF, Chapman ER, Jackson MB (2001). Synaptotagmin modulation of fusion pore kinetics in regulated exocytosis of dense-core vesicles. Science 294, 1111–1115.
Wang CT, Lu JC, Bai J, Chang PY, Martin TF, Chapman ER, Jackson MB (2003). Different domains of synaptotagmin control the choice between kiss-and-run and full fusion. Nature 424, 943–947.
Wang P, Chicka MC, Bhalla A, Richards DA, Chapman ER (2005). Synaptotagmin VII is targeted to secretory organelles in PC12 cells, where it functions as a high-affinity calcium sensor. Mol Cell Biol 25, 8693–8702.
Whim MD (2006). Near simultaneous release of classical and peptide cotransmitters from chromaffin cells. J Neurosci 26, 6637–6642.
Willig KI, Rizzoli SO, Westphal V, Jahn R, Hell SW (2006). STED microscopy reveals that synaptotagmin remains clustered after synaptic vesicle exocytosis. Nature 440, 935–939.
Winkler H, Apps DK, Fischer-Colbrie R (1986). The molecular function of adrenal chromaffin granules: established facts and unresolved topics. Neuroscience 18, 261–290.
Zhang X, Kim-Miller MJ, Fukuda M, Kowalchyk JA, Martin TF (2002). Ca^{2+}-dependent synaptotagmin binding to SNAP-25 is essential for Ca^{2+}-triggered exocytosis. Neuron 34, 599–611.
Zhang Z, Bhalla A, Dean C, Chapman ER, Jackson MB (2009a). Synaptotagmin IV: a multifunctional regulator of peptidergic nerve terminals. Nat Neurosci 12, 163–171.
Zhang Z, Hui E, Chapman ER, Jackson MB (2009b). Phosphatidylserine regulation of Ca^{2+}-triggered exocytosis and fusion pores in PC12 cells. Mol Biol Cell 20, 5086–5095.
Zhang Z, Hui E, Chapman ER, Jackson MB (2010a). Regulation of exocytosis and fusion pores by synaptotagmin-effector interactions. Mol Biol Cell 21, 2821–2831.
Zhang Z, Jackson MB (2008). Temperature dependence of fusion kinetics and fusion pores in Ca^{2+}-triggered exocytosis from PC12 cells. J Gen Physiol 131, 117–124.
Zhang Z, Jackson MB (2010). Membrane bending energy and fusion pore kinetics in Ca(2+)-triggered exocytosis. Biophys J 98, 2524–2534.
Zhang Z, Zhang Z, Jackson MB (2010b). Synaptotagmin IV modulation of vesicle size and fusion pores in PC12 cells. Biophys J 98, 968–978.
Zhou Z, Misler S (1995). Action potential-induced quantal secretion of catecholamines from rat adrenal chromaffin cells. J Biol Chem 270, 3498–3505.
Zhou Z, Misler S, Chow RH (1996). Rapid fluctuations in transmitter release from single vesicles in bovine adrenal chromaffin cells. Biophys J 70, 1543–1552.
Zhu D, Zhou W, Liang T, Yang F, Zhang RY, Wu ZX, Xu T (2007). Synaptotagmin I and IX function redundantly in controlling fusion pore of large dense core vesicles. Biochem Biophys Res Commun 361, 922–927.